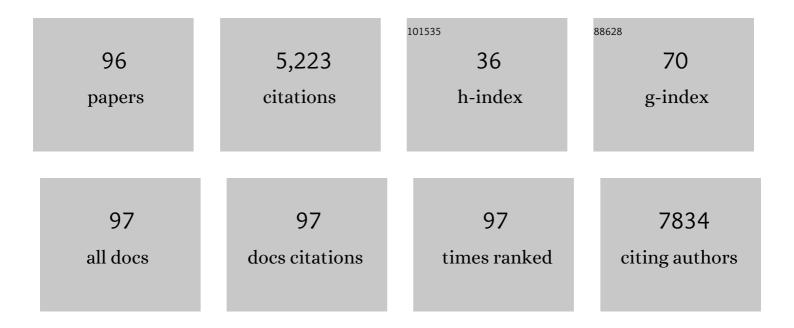
List of Publications by Year in descending order

Source: https://exaly.com/author-pdf/1114728/publications.pdf Version: 2024-02-01



LINFENC FEL

#	Article	IF	CITATIONS
1	High-Quality Luminescent Tellurium Nanowires of Several Nanometers in Diameter and High Aspect Ratio Synthesized by a Poly (Vinyl Pyrrolidone)-Assisted Hydrothermal Process. Langmuir, 2006, 22, 3830-3835.	3.5	296
2	Harvesting the Vibration Energy of BiFeO ₃ Nanosheets for Hydrogen Evolution. Angewandte Chemie - International Edition, 2019, 58, 11779-11784.	13.8	277
3	Synthesis of Uniform Te@Carbon-Rich Composite Nanocables with Photoluminescence Properties and Carbonaceous Nanofibers by the Hydrothermal Carbonization of Glucose. Chemistry of Materials, 2006, 18, 2102-2108.	6.7	253
4	Valence Engineering via Selective Atomic Substitution on Tetrahedral Sites in Spinel Oxide for Highly Enhanced Oxygen Evolution Catalysis. Journal of the American Chemical Society, 2019, 141, 8136-8145.	13.7	220
5	Direct TEM observations of growth mechanisms of two-dimensional MoS2 flakes. Nature Communications, 2016, 7, 12206.	12.8	179
6	NaNbO ₃ â€(Bi _{0.5} Li _{0.5})TiO ₃ Leadâ€Free Relaxor Ferroelectric Capacitors with Superior Energyâ€Storage Performances via Multiple Synergistic Design. Advanced Energy Materials, 2021, 11, 2101378.	19.5	170
7	Highly Efficient Porous Carbon Electrocatalyst with Controllable Nâ€Species Content for Selective CO ₂ Reduction. Angewandte Chemie - International Edition, 2020, 59, 3244-3251.	13.8	167
8	Seleniumâ€Doped Black Phosphorus for Highâ€Responsivity 2D Photodetectors. Small, 2016, 12, 5000-5007.	10.0	156
9	Piezoelectrically/pyroelectrically-driven vibration/cold-hot energy harvesting for mechano-/pyro- bi-catalytic dye decomposition of NaNbO3 nanofibers. Nano Energy, 2018, 52, 351-359.	16.0	151
10	Carbon nanofibers: Synthesis, characterization, and electrochemical properties. Carbon, 2006, 44, 828-832.	10.3	146
11	Synergistic strain engineering of perovskite single crystals for highly stable and sensitive X-ray detectors with low-bias imaging and monitoring. Nature Photonics, 2022, 16, 575-581.	31.4	138
12	Shape-Controlled Synthesis of 3D and 1D Structures of CdS in a Binary Solution withL-Cysteine's Assistance. Chemistry - A European Journal, 2007, 13, 3076-3081.	3.3	137
13	High-Yield Synthesis of NiO Nanoplatelets and Their Excellent Electrochemical Performance. Crystal Growth and Design, 2006, 6, 2163-2165.	3.0	132
14	Photoflexoelectric effect in halide perovskites. Nature Materials, 2020, 19, 605-609.	27.5	132
15	Tailoring Anisotropic Li-Ion Transport Tunnels on Orthogonally Arranged Li-Rich Layered Oxide Nanoplates Toward High-Performance Li-Ion Batteries. Nano Letters, 2017, 17, 1670-1677.	9.1	128
16	Flexoelectric materials and their related applications: A focused review. Journal of Advanced Ceramics, 2019, 8, 153-173.	17.4	127
17	Highly Responsive Room-Temperature Hydrogen Sensing of α-MoO ₃ Nanoribbon Membranes. ACS Applied Materials & Interfaces, 2015, 7, 9247-9253.	8.0	125
18	Graphene/Sulfur Hybrid Nanosheets from a Spaceâ€Confined "Sauna―Reaction for Highâ€Performance Lithium–Sulfur Batteries. Advanced Materials, 2015, 27, 5936-5942.	21.0	124

#	Article	IF	CITATIONS
19	A rectification-free piezo-supercapacitor with a polyvinylidene fluoride separator and functionalized carbon cloth electrodes. Journal of Materials Chemistry A, 2015, 3, 14963-14970.	10.3	118
20	Visible Light Responsive Perovskite BiFeO ₃ Pills and Rods with Dominant {111} _c Facets. Crystal Growth and Design, 2011, 11, 1049-1053.	3.0	115
21	Tetra-heteroatom self-doped carbon nanosheets derived from silkworm excrement for high-performance supercapacitors. Journal of Power Sources, 2018, 379, 74-83.	7.8	101
22	Engineering hetero-epitaxial nanostructures with aligned Li-ion channels in Li-rich layered oxides for high-performance cathode application. Nano Energy, 2017, 35, 271-280.	16.0	99
23	Commercial Dacron cloth supported Cu(OH) ₂ nanobelt arrays for wearable supercapacitors. Journal of Materials Chemistry A, 2016, 4, 14781-14788.	10.3	78
24	Harvesting the Vibration Energy of BiFeO ₃ Nanosheets for Hydrogen Evolution. Angewandte Chemie, 2019, 131, 11905-11910.	2.0	75
25	Synthesis of Bismuth Ferrite Nanoparticles via a Wet Chemical Route at Low Temperature. Journal of Nanomaterials, 2011, 2011, 1-6.	2.7	73
26	Synthesis of copper/cross-linked poly(vinyl alcohol) (PVA) nanocables via a simple hydrothermal route. Journal of Materials Chemistry, 2006, 16, 101-105.	6.7	72
27	A FeCO3Precursor-Based Route to Microsized Peanutlike Fe3O4. Crystal Growth and Design, 2007, 7, 430-434.	3.0	69
28	Engineering Nanostructured <scp> <scp>Bi₂WO₆–TiO₂</scp> </scp> Toward Effective Utilization of Natural Light in Photocatalysis. Journal of the American Ceramic Society, 2011, 94, 4157-4161.	3.8	68
29	Bias-switchable negative and positive photoconductivity in 2D FePS ₃ ultraviolet photodetectors. Nanotechnology, 2018, 29, 244001.	2.6	67
30	Fullerene-Anchored Core-Shell ZnO Nanoparticles for Efficient and Stable Dual-Sensitized Perovskite Solar Cells. Joule, 2019, 3, 417-431.	24.0	61
31	Electrospun Bismuth Ferrite Nanofibers for Potential Applications in Ferroelectric Photovoltaic Devices. ACS Applied Materials & Interfaces, 2015, 7, 3665-3670.	8.0	55
32	Large-area color controllable remote carbon white-light light-emitting diodes. Carbon, 2015, 85, 344-350.	10.3	49
33	van der Waals epitaxy of Al-doped ZnO film on mica as a flexible transparent heater with ultrafast thermal response. Applied Physics Letters, 2018, 112, .	3.3	43
34	Fabrication of completely interface-engineered Ni(OH)2/rGO nanoarchitectures for high-performance asymmetric supercapacitors. Applied Surface Science, 2018, 460, 65-73.	6.1	38
35	FeCo alloy catalysts promoting polysulfide conversion for advanced lithium–sulfur batteries. Journal of Energy Chemistry, 2020, 49, 339-347.	12.9	38
36	Controllable in situ synthesis of epsilon manganese dioxide hollow structure/RGO nanocomposites for high-performance supercapacitors. Nanoscale, 2016, 8, 1854-1860.	5.6	37

#	Article	IF	CITATIONS
37	Te@Cross-Linked PVA Coreâ^'Shell Structures Synthesized by a One-Step Synergistic Softâ^'Hard Template Process. Crystal Growth and Design, 2006, 6, 607-611.	3.0	36
38	The Fabrication and Characterization of Single-Crystalline Selenium Nanoneedles. Crystal Growth and Design, 2006, 6, 1711-1716.	3.0	36
39	Mechanism study on extraordinary room-temperature CO sensing capabilities of Pd-SnO2 composite nanoceramics. Sensors and Actuators B: Chemical, 2019, 285, 49-55.	7.8	36
40	Highly entangled carbon nanoflakes on Li ₃ V ₂ (PO ₄) ₃ microrods for improved lithium storage performance. RSC Advances, 2013, 3, 1297-1301.	3.6	32
41	Observable Two-Step Nucleation Mechanism in Solid-State Formation of Tungsten Carbide. ACS Nano, 2019, 13, 681-688.	14.6	32
42	Self-Doped Rutile Titania with High Performance for Direct and Ultrafast Assay of H ₂ O ₂ . ACS Applied Materials & Interfaces, 2013, 5, 12784-12788.	8.0	30
43	Plasmon-induced trap filling at grain boundaries in perovskite solar cells. Light: Science and Applications, 2021, 10, 219.	16.6	30
44	An ultra-long and low junction-resistance Ag transparent electrode by electrospun nanofibers. RSC Advances, 2016, 6, 91641-91648.	3.6	29
45	Atomic-Scale Mechanism on Nucleation and Growth of Mo ₂ C Nanoparticles Revealed by in Situ Transmission Electron Microscopy. Nano Letters, 2016, 16, 7875-7881.	9.1	28
46	Graphene nanocluster decorated niobium oxide nanofibers for visible light photocatalytic applications. Journal of Materials Chemistry A, 2014, 2, 8190.	10.3	27
47	Epitaxial Regeneration of Spent Graphite Anode Material by an Eco-friendly In-Depth Purification Route. ACS Sustainable Chemistry and Engineering, 2021, 9, 16192-16202.	6.7	27
48	Direct observation of carbon nanostructure growth at liquid–solid interfaces. Chemical Communications, 2014, 50, 826-828.	4.1	25
49	A new low-temperature solution route to Aurivillius-type layered oxyfluoride perovskites Bi2MO5F (M) Tj ETQq1	1 0,78431 20.2	4 rgBT /Over 24
50	Core–shell Fe ₃ O ₄ @SiO ₂ @HNbMoO ₆ nanocomposites: new magnetically recyclable solid acid for heterogeneous catalysis. Journal of Materials Chemistry A, 2015, 3, 3456-3464.	10.3	23
51	Flexoelectric behavior in PIN-PMN-PT single crystals over a wide temperature range. Applied Physics Letters, 2017, 111, .	3.3	23
52	Tailoring Phase Purity in the 2D/3D Perovskite Heterostructures Using Lattice Mismatch. ACS Energy Letters, 2022, 7, 550-559.	17.4	23
53	Synthesis and electrochemical properties of nanocrystalline V2O5 flake via a citric acid-assistant sol–gel method. Journal of Crystal Growth, 2005, 281, 463-467.	1.5	21
54	Stable 4 V-class bicontinuous cathodes by hierarchically porous carbon coating on Li ₃ V ₂ (PO ₄) ₃ nanospheres. Nanoscale, 2014, 6, 12426-12433.	5.6	20

#	Article	IF	CITATIONS
55	Highly Efficient Porous Carbon Electrocatalyst with Controllable Nâ€Species Content for Selective CO 2 Reduction. Angewandte Chemie, 2020, 132, 3270-3277.	2.0	20
56	Preparation of α-MnO2 nanowires through a γ-MnOOH precursor route. Materials Letters, 2007, 61, 1785-1788.	2.6	17
57	Electrospinning preparation and high-temperature superconductivity of YBa2Cu3O7-x nanotubes. Journal of Materials Science, 2013, 48, 3985-3990.	3.7	17
58	Atomic Steps Induce the Aligned Growth of Ice Crystals on Graphite Surfaces. Nano Letters, 2020, 20, 8112-8119.	9.1	17
59	Effect of Thickness on the Optical and Electrical Properties of ITO/Au/ITO Sandwich Structures. ACS Applied Materials & Interfaces, 2020, 12, 13437-13446.	8.0	17
60	Enhancement of electrochemical capacitive properties based on complementation of morphologies. Electrochimica Acta, 2012, 81, 1-7.	5.2	16
61	Epitaxial growth and interface strain coupling effects in manganite film/piezoelectric-crystal multiferroic heterostructures. Materials Chemistry and Physics, 2012, 133, 42-46.	4.0	16
62	Multifunctional NiTiO ₃ nanocoating fabrication based on the dual-Kirkendall effect enabling a stable cathode/electrolyte interface for nickel-rich layered oxides. Journal of Materials Chemistry A, 2018, 6, 2643-2652.	10.3	16
63	Thermodynamically Metal Atom Trapping in Van der Waals Layers Enabling Multifunctional 3D Carbon Network. Advanced Functional Materials, 2020, 30, 2002626.	14.9	15
64	Rational Design and in-situ Synthesis of Ultra-Thin β-Ni(OH)2 Nanoplates for High Performance All-Solid-State Flexible Supercapacitors. Frontiers in Chemistry, 2020, 8, 602322.	3.6	14
65	Self-Poisoning by C ₂ Products in CO ₂ Photoreduction Using a Phosphorus-Doped Carbon Nitride with Nitrogen Vacancies. ACS Sustainable Chemistry and Engineering, 2022, 10, 5758-5769.	6.7	14
66	Multiarmed Tubular Selenium with Potentially Unique Electrical Properties: Solution-Phase Synthesis and First-Principles Calculation. Small, 2007, 3, 101-105.	10.0	13
67	Three-dimensional macroporous graphene monoliths with entrapped MoS ₂ nanoflakes from single-step synthesis for high-performance sodium-ion batteries. RSC Advances, 2018, 8, 2477-2484.	3.6	13
68	Flexoelectric fatigue in (K,Na,Li)(Nb,Sb)O3 ceramics. Applied Physics Letters, 2018, 113, .	3.3	13
69	Applications of ESEM on Materials Science: Recent Updates and a Look Forward. Small Methods, 2020, 4, 1900588.	8.6	12
70	Controllable Thermal Oxidation and Photoluminescence Enhancement in Quasi-1D van der Waals ZrS ₃ Flakes. ACS Applied Electronic Materials, 2020, 2, 3756-3764.	4.3	12
71	A facial strategy to synthesize Co3O4 hollow tube nanoarray with enhanced supercapacitive performance. Journal of Energy Storage, 2021, 34, 102169.	8.1	12
72	Large-scale synthesis of Li3V2(PO4)3@C composites by a modified carbothermal reduction method as cathode material for lithium-ion batteries. RSC Advances, 2017, 7, 25422-25428.	3.6	11

#	Article	IF	CITATIONS
73	Magnetotransport and magnetic properties of the layered noncollinear antiferromagnetic Cr ₂ Se ₃ single crystals. Journal of Physics Condensed Matter, 2020, 32, 475801.	1.8	11
74	Effect of post-annealing on laser-ablation deposited WS 2 thin films. Vacuum, 2018, 152, 239-242.	3.5	9
75	<i>In Situ</i> Observation of Ice Formation from Water Vapor by Environmental SEM. Crystal Growth and Design, 2018, 18, 6602-6608.	3.0	9
76	Tailoring carrier dynamics in inverted mesoporous perovskite solar cells with interface-engineered plasmonics. Journal of Materials Chemistry A, 2021, 9, 2394-2403.	10.3	9
77	Visualization of Bubble Nucleation and Growth Confined in 2D Flakes. Small, 2021, 17, e2103301.	10.0	9
78	Preparation of Semiconductor/Polymer Coaxial Nanocables by a Facile Solution Process. European Journal of Inorganic Chemistry, 2006, 2006, 207-212.	2.0	8
79	Superior acidic catalytic activity and stability of Fe-doped HTaWO6 nanotubes. Nanoscale, 2017, 9, 11126-11136.	5.6	8
80	An approach through steam to form sulfur nanoparticles for lithium sulfur batteries. Electrochemistry Communications, 2021, 125, 107010.	4.7	8
81	Few-Layered MnAl ₂ S ₄ Dielectrics for High-Performance van der Waals Stacked Transistors. ACS Applied Materials & Interfaces, 2022, 14, 25920-25927.	8.0	8
82	Room-temperature large magnetic-dielectric coupling in new phase anatase VTiO4. Chemical Communications, 2013, 49, 10462.	4.1	7
83	Evidencing the structural conversion of hydrothermally synthesized titanate nanorods by in situ electron microscopy. Journal of Materials Chemistry A, 2017, 5, 3786-3791.	10.3	7
84	A Hierarchically Porous Hollow Structure of Layered Bi ₂ TiO ₄ F ₂ for Efficient Photocatalysis. European Journal of Inorganic Chemistry, 2017, 2017, 1892-1899.	2.0	7
85	Silkworm Excrement Derived Inâ€situ Coâ€doped Nanoporous Carbon as Confining Sulfur Host for Lithium Sulfur Batteries. ChemistrySelect, 2019, 4, 5678-5685.	1.5	7
86	Multistep nucleation visualized during solid-state crystallization. Materials Horizons, 2022, 9, 1670-1678.	12.2	6
87	Epitaxial growth and rectification characteristics of double perovskite oxide La2NiMnO6 films on Nb-SrTiO3 single crystal substrates. Thin Solid Films, 2011, 519, 6148-6150.	1.8	5
88	Photocatalytically Active YBa ₂ Cu ₃ O _{7â^'<i>x</i>} Nanoparticles Synthesized via a Soft Chemical Route. Journal of Nanomaterials, 2015, 2015, 1-5.	2.7	5
89	Simultaneous engineering on absorption window and transportation geometry of graphene-based foams toward high-performance solar steam generator. Applied Surface Science, 2022, 599, 154021.	6.1	5
90	Modulating Magnetism in Ferroelectric Polymer-Gated Perovskite Manganite Films with Moderate Gate Pulse Chains. ACS Applied Materials & Interfaces, 2020, 12, 56541-56548.	8.0	4

#	Article	IF	CITATIONS
91	<i>In situ</i> observations for growth kinetics of water droplets on Bambusa multiplex leaves. Applied Physics Letters, 2019, 114, .	3.3	3
92	Negative Coriolis effect in piezoelectric metamaterials. Journal of Alloys and Compounds, 2019, 801, 262-266.	5.5	2
93	Visualization of Bubble Nucleation and Growth Confined in 2D Flakes (Small 39/2021). Small, 2021, 17, 2170205.	10.0	1
94	Atomic mechanism for the transformation of amorphous carbon film to graphene on Cu substrate. Computational Materials Science, 2022, 203, 111145.	3.0	1
95	High-Temperature Flexible Transparent Heater for Rapid Thermal Annealing of Thin Films. Physical Review Applied, 2022, 17, .	3.8	1
96	Atomic insights in crystallization of liquid Cu on single crystal Ta and amorphous Ta. Materials Research Express, 2020, 7, 015201.	1.6	0